Optical absorption in the soliton model for polyacetylene

Michielsen, Kristel; de Raedt, Hans

Published in:
Modern Physics Letters B

DOI:
10.1142/S0217984996000511

Publication date:
1996

Modern Physics Letters B, Vol. 10, No. 10 (1996) 467–474

OPTICAL ABSORPTION IN THE SOLITON MODEL FOR POLYACETYLENE

KRISTEL MICHIELSEN and HANS DE RAEDT

Institute for Theoretical Physics and Materials Science Centre, University of Groningen, Nijenborgh 4, NL-9747 AG Groningen, The Netherlands

Received 9 April 1996

A quantum molecular dynamics technique is used to compute the optical absorption at room-temperature for the soliton model for trans-polyacetylene in the semiclassical limit. Our simulation data for the optical absorption for dopant concentrations below 6% are in good agreement with experiment.

The proposal[1–3] that solitons play an important role in the physics of trans-polyacetylene has led to considerable theoretical and experimental interest in the system.[4–6] Direct evidence for the existence of charged solitons in trans-polyacetylene at dilute doping levels comes from optical absorption experiments.[7] Within the soliton model there is a localized state associated with each soliton which, due to the electron-hole symmetry of the model, is precisely located at midgap.[1–6] Therefore a midgap peak is expected to appear in the optical absorption upon doping with an intensity proportional to the dopant concentration. These general features are observed in several optical absorption experiments.[7–9]

Because of the importance of the optical absorption experiments in providing direct evidence for the existence of charged solitons in doped trans-polyacetylene, a number of zero-temperature calculations of the optical absorption for the soliton model were made to make a comparison between theory and experiment.[7,10–12] All these calculations are for dimerized chains (Peierls systems) in the presence of no or one single soliton[7,10–12] and/or in the low density limit for solitons.[10,11] More recently, the frequency and temperature dependence of the optical conductivity for a half-filled dimerized chain has been studied and comparison with experimental results on trans-polyacetylene was made.[13]

The purpose of this work is to present the results of the optical absorption spectra for the Su–Schrieffer–Heeger (SSH) model[1–6] at room-temperature and for all relevant dopant concentrations and to compare the experimental results with the

PACS Nos.: 71.10.+x, 61.20.Ja, 71.38.+i

theoretical predictions of the SSH model. The SSH model Hamiltonian reads[1–6]

$$\mathcal{H} = -\sum_i \sum_s \left[t - \alpha\left(u_{i+1} - u_i\right)\right]\left(c^+_{i,s}c_{i+1,s} + c^+_{i+1,s}c_{i,s}\right) - \mu \sum_i \sum_s n_{i,s} + \frac{1}{2M}\sum_i p_i^2 + \frac{K}{2}\sum_i \left(u_{i+1} - u_i\right)^2 , \tag{1}$$

where $c^+_{i,s}$ and $c_{i,s}$ are the creation and annihilation operators, respectively, for a π-electron with spin $s = \uparrow, \downarrow$ at the ith CH group, $n_{i,s}$ denotes the number operator at group i, μ is the chemical potential which fixes the number of π-electrons, u_i is the coordinate describing the displacement of the ith CH group along the molecular symmetry axis, p_i is the corresponding momentum, t is the hopping integral for the undimerized chain, α is the electron–phonon coupling constant, K is the effective σ-spring constant and M is the total mass of the CH group.[1–6] We used the following set of model parameters which is often adopted in model calculations of polyacetylene[2–6]: $t = 2.5$ eV, $\alpha = 4.1$ eV/Å, $K = 21$ eV/Å^2 and $M = 3145$ eV^{-1}/Å^2. In this work we will only consider even-site rings of length L.

For numerical purposes it is useful to rewrite Hamiltonian (1) as[14] $\mathcal{H} = \mathcal{H}_1 + \mathcal{H}_2$ where

$$\mathcal{H}_1 = \sum_{i,j}\sum_s c^+_{i,s} M_{ij}(\{u_i\}) c_{j,s} + \frac{K}{2}\sum_i \left(u_{i+1} - u_i\right)^2 , \tag{2a}$$

$$\mathcal{H}_2 = \frac{1}{2M}\sum_i p_i^2 , \tag{2b}$$

and $M_{ii}(\{u_i\}) = -\mu$, $M_{ij}(\{u_i\}) = -t + \alpha(u_j - u_i)$ for i, j nearest neighbors, and $M_{ij}(\{u_i\}) = 0$ otherwise. In the semiclassical limit[15] the grand-canonical partition function for model (2) can be written as

$$Z = \mathrm{Tr}\, e^{-\beta\mathcal{H}_1} e^{-\beta\mathcal{H}_2} = \left(\frac{2M\pi}{\beta}\right)^{L/2} \int_{\{u_i\}} e^{-\beta E(\{u_i\})} \mathrm{tr}\, e^{-\beta\mathcal{H}_1} , \tag{3}$$

where β denotes the inverse temperature and $E(\{u_i\}) = K\sum_i \left(u_{i+1} - u_i\right)^2/2$ is the potential energy of the lattice degrees of freedom. In the semiclassical approximation the electrons are treated quantum mechanically whereas the displacements may be regarded as classical degrees of freedom, a good starting point for the description of the electronic properties of trans-polyacetylene.[1–6]

Since $\mathcal{H}$ is a quadratic form in the fermionic degrees of freedom the trace over the fermions can be performed analytically, yielding for the partition function the exact expression

$$Z = \int_{\{u_i\}} \rho(\{u_i\}) = \left(\frac{2M\pi}{\beta}\right)^{L/2} \int_{\{u_i\}} e^{-\beta E(\{u_i\})} \left[\det\left(1 + e^{-\beta M(\{u_i\})}\right)\right]^2 , \tag{4}$$

The weight $\rho(\{u_i\})$ of the configuration $\{u_i\}$ is strictly positive and can be used directly in a Metropolis Monte Carlo simulation of the variables $\{u_i\}$. Our algorithm

samples the full phase space and is, by construction, free of minus-sign problems or numerical instabilities.[16] The latter enables us to cover a much wider range of temperatures than the one which is usually accessible to other Quantum Monte Carlo methods.[17]

Time-dependent quantities, such as the optical absorption, can be calculated directly, in the real-time domain, without invoking procedures[17] for extrapolating imaginary-time data to the real-time axis. When a pulse of electric field is applied in the direction of the molecular symmetry axis, the linear response in this direction is given by $\sigma(\tau) = -i\langle[P(-\tau), J]\rangle$, where $J = i[\mathcal{H}, P] = i\sum_{l,s}(-t + \alpha(u_{l+1} - u_l)) \times (c^+_{l,s}c_{l+1,s} - c^+_{l+1,s}c_{l,s})$ is the current operator for the SSH model and $P = \sum_l ln_l$ is the polarization operator. The time evolution of the polarization operator is defined as $P(\tau) = e^{i\tau\mathcal{H}}Pe^{-i\tau\mathcal{H}}$. In the semiclassical limit $\sigma(\tau) = -i\langle[e^{-i\tau\mathcal{H}_1}Pe^{i\tau\mathcal{H}_1}, J]\rangle = -i\langle[P, e^{i\tau\mathcal{H}_1}Je^{-i\tau\mathcal{H}_1}]\rangle$.

The Kubo formula for the optical conductivity reads[18]

$$\sigma(\omega) = \lim_{\epsilon\to 0}\frac{i}{\omega + i\epsilon}\left\{-\sum_{l,s}\left\langle\left[lc^+_{l,s}c_{l,s}, J\right]\right\rangle + \int_0^\infty e^{i\omega\tau}e^{-\epsilon\tau}\langle[J, J(\tau)]\rangle d\tau\right\}. \quad (5)$$

The time evolution of the current operator $J(\tau) = e^{i\tau\mathcal{H}_1}Je^{-i\tau\mathcal{H}_1}$ can be worked out analytically, yielding

$$J(\tau) = i\sum_{i,j,k}\sum_s \kappa_{i,i+1}\left[\left(e^{i\tau M}\right)_{j,i}\left(e^{-i\tau M}\right)_{i+1,k}c^+_{j,s}c_{k,s} - \left(e^{i\tau M}\right)_{k,i+1}\left(e^{-i\tau M}\right)_{i,j}c^+_{k,s}c_{j,s}\right], \quad (6)$$

with $\kappa_{i,i+1} = -t + \alpha(u_{i+1} - u_i)$. The analytical expression for the commutator appearing in (5) is given by

$$[J, J(\tau)] = -\sum_{i,j}\kappa_{i,i+1}\kappa_{j,j+1}(F_{i,i+1,j,j+1} - F_{i,i+1,j+1,j} - F_{i+1,i,j,j+1} + F_{i+1,i,j+1,j}), \quad (7)$$

where

$$F_{i,i+1,j,j+1} = \sum_k\sum_s\left\{\left(e^{i\tau M}\right)_{i+1,j}\left(e^{-i\tau M}\right)_{j+1,k}c^+_{i,s}c_{k,s} - \left(e^{i\tau M}\right)_{k,j+1}\left(e^{-i\tau M}\right)_{j,i+1}c^+_{k,s}c_{i,s}\right\}. \quad (8)$$

Making use of the particular form of the Hamiltonian (2), the expectation value on (6) can be worked out analytically. The resulting expression for the integrand in (6) is used to sample the current-current correlation function for a set of τ-values (typically 512). After collecting all data, application of a Fast Fourier Transform yields the frequency-dependent conductivity. The computation time per τ-value increases with the third power of L, effectively limiting the system size that we can

study to $L \leq 256$. Disregarding the statistical errors (which are too small to be visible on the figures presented below) the results for model (3) in the semiclassical limit are, for all practical purposes exact.[16]

The conductivity (6) contains a delta function $D\delta(\omega)$ where D is called the Drude weight. As discussed originally by Kohn[19] and more recently by Shastry and Sutherland[20] and by Scalapino *et al.*,[21] D serves as a direct and sensitive measure of a metal-insulator transition. If $D = 0$ the system is insulating and otherwise it is conducting.

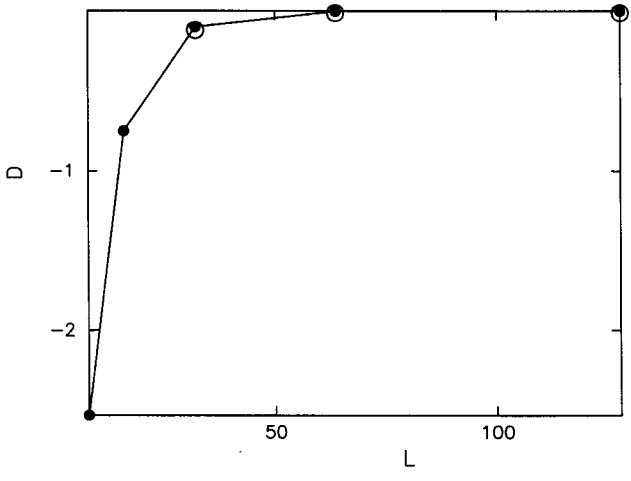

Fig. 1. Drude weight D as a function of the number of sites L. Bullets: D calculated from (11) with $u_0 = 0.04$ Å, circles: Quantum molecular dynamics results for $T = 2.9$ K, corresponding to $\beta t = 10000$. The line is a guide to the eye.

First we demonstrate that our method reproduces the optical conductivity and the insulating feature of the half-filled system at zero-temperature. At half-filling the configuration $\{u_i\}$ with equal spacing between the CH groups is unstable with respect to a dimerization distortion, the Peierls instability,[22] in which adjacent CH groups move toward each other. The Hamiltonian which describes a completely dimerized chain is given by

$$H = t_+ \sum_{j,s} \left(c^+_{2j+1,s} c_{2j+2,s} + h.c.\right) + t_- \sum_{j,s} \left(c^+_{2j+2,s} c_{2j+3,s} + \text{h.c.}\right) , \tag{9}$$

where $t_\pm = t \pm 2\alpha u_0$ and $u_0 = |\sum_i (-1)^i \langle u_i \rangle| / 2L$ is the distortion parameter. The optical conductivity for model (9) can be worked out analytically, yielding

$$\sigma(\omega) = \lim_{\epsilon \to 0} \frac{1}{\omega + i\epsilon} \left\{ -\sum_k \epsilon_k + 4 \sum_k \frac{\left(t_+^2 - t_-^2\right)^2}{\epsilon_k \left(\epsilon - i\omega\right)^2 + 4\epsilon_k^3} \right\} , \tag{10}$$

where $\epsilon_k = -\sqrt{t_+^2 + t_-^2 + 2t_+ t_- \cos(4\pi k/L)}$. Extraction of the Drude weight gives

for the dimerized chain

$$D = -\sum_k \epsilon_k + \left(t_+^2 - t_-^2\right)^2 \sum_k \frac{1}{\epsilon_k^3}. \tag{11}$$

In Fig. 1 the Drude weight is shown as a function of system size. Our quantum molecular dynamics results (circles) for $\beta t = 10000$ (or $T = 2.9K$) agree very well with the results obtained from (11) (bullets). The Drude weight for $L = 4n$-site rings is negative and goes to zero as the number of lattice sites increases. Systems with more than 64 sites are needed to obtain $D = 0$, as is expected for a semiconductor at zero-temperature. Negative values for D are also seen in short half-filled Hubbard rings with $4n$-sites.[23] Our simulation technique also reproduces the exact values of $\sigma(\omega)$ as given by (10) (data not shown).

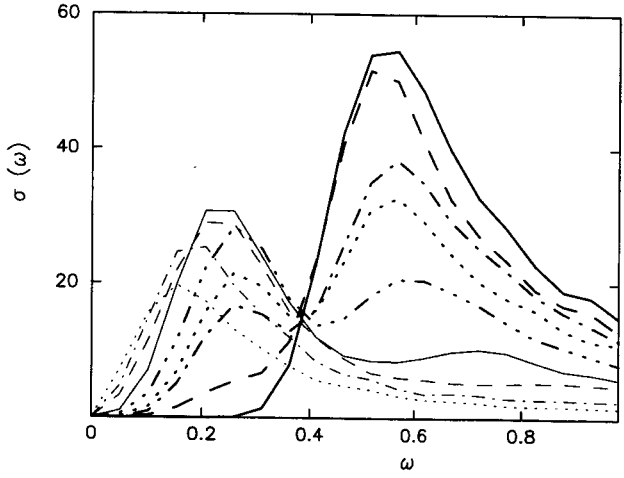

Fig. 2. Optical absorption $\sigma(\omega)$ for a ring of 128 sites for various dopant concentrations. Thick solid line: $y = 0$, thick dashed line: $y = 0.008$, thick dash-dotted line: $y = 0.016$, thick dotted line: $y = 0.02$, thick dash-triple dotted line: $y = 0.031$, thin solid line: $y = 0.047$, thin dashed line: $y = 0.063$, thin dash-dotted line: $y = 0.078$, thin dotted line: $y = 0.109$. ω is measured in units of $t = 2.5$ eV.

The optical absorption spectra $\sigma(\omega)$ at room-temperature (in practice we set $T = 290$ K, corresponding to $\beta t = 100$) for various dopant concentrations $y = 1 - n$, where n is the density of electrons in the chain are depicted in Fig. 2 for rings of 128 sites. For the undoped case (thick solid line) $\sigma(\omega)$ shows an interband transition peak at $\omega = 1.42 \pm 0.13$ eV. Upon doping and for dopant concentrations below 6%, a midgap absorption peak appears at $\omega = 0.64 \pm 0.13$ eV. The intensity of the midgap absorption peak comes from the interband transition over the whole spectral range. The optical conductivities for different dopant concentrations ($y < 0.06$) cross in one point (the isosbestic point) at $\omega = 1.03 \pm 0.13$ eV. These features are also observed experimentally.[7–9] However, in comparison with experiment our peak positions and our isosbestic point are located at somewhat lower

energies. In Fig. 3 we show the intensity of the midgap absorption peak (optical density) as a function of dopant concentration for $y < 0.06$. Our numerical results (bullets) indicate that for $y < 0.031$ the intensity of the midgap absorption peak increases linearly with the dopant concentration. In the intermediate doping regime $0.031 < y < 0.06$, the doping dependence of the intensity of the midgap absorption changes. Similar behavior is seen in the optical absorption measurements of Feldblum *et al.*[8] (circles). However, our results show that for $0.031 < y < 0.06$ the midgap absorption peak becomes higher than the interband transition peak, in disagreement with some experiments[7–9] but in agreement with others.[24] In the heavily doped regime ($y > 0.06$) the low-energy absorption shrinks with increasing dopant concentration and shifts toward lower energy, while the interband transition has completely disappeared, as seen in Fig. 2.

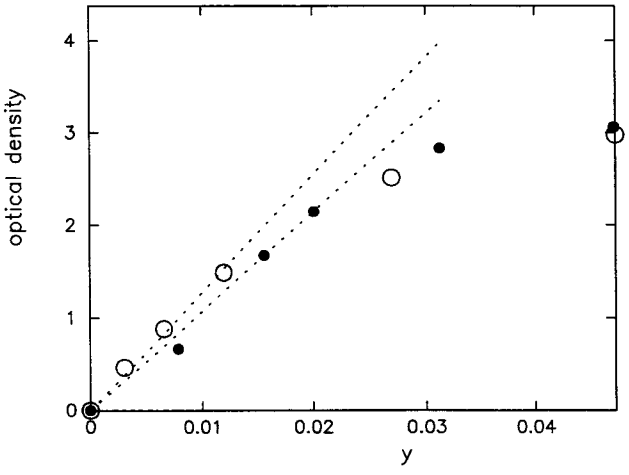

Fig. 3. Concentration dependence of the midgap optical absorption (arbitrary units). Circles: Experimental data.[8] Bullets: Simulation data taken from Fig. 1. The dotted lines are a guide to the eye.

At low temperature (e.g. $T = 2.9$ K or $\beta t = 10000$) only states with an even number of electrons are thermodynamically stable in a system containing an even number of sites. Moderate doping ($y < 0.031$) results in the creation of soliton-antisoliton pairs only.[16] At room temperature this is no longer the case: The system is thermodynamically stable with respect to the removal of a single (or odd number of) electron(s), independent of the filling. Our calculations show that for moderate doping and an odd number of electrons, the thermodynamically relevant states consist of configurations with a single polaron and/or soliton-antisoliton pairs, an example being shown in Fig. 4. From Fig. 1 it is clear that the optical conductivity for systems containing a polaron (see the thick dashed and thick dotted line) does not show any extra features compared to the conductivity of systems without a polaron. Further evidence for this is provided by the data shown in Fig. 2 (second and fourth bullet, counting from left to right). Our results for the density of states

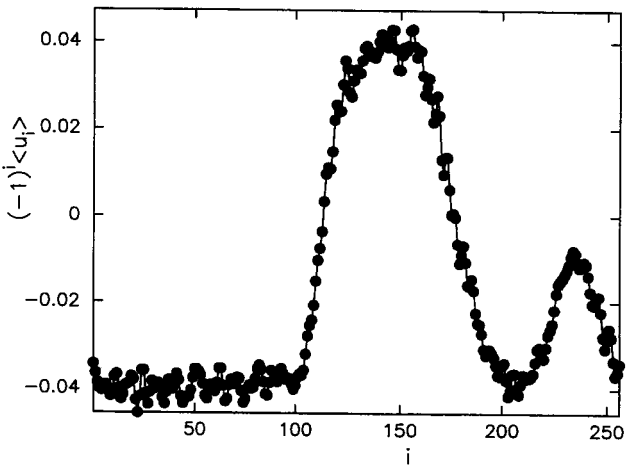

Fig. 4. Lattice distortion for a ring of 256 sites for $y = 0.012$ (3 electrons removed from the half-filled ring). The line is a guide to the eye.

(not shown) indicate that the polaron and the soliton-antisoliton pairs contribute to the weight at $\omega = 0$.[5]

Acknowledgments

This work is partially supported by a Human Capital and Mobility grant and the "Stichting voor Fundamenteel Onderzoek der Materie (FOM)", which is financially supported by the "Nederlandse Organisatie voor Wetenschappelijk Onderzoek (NWO)" and a supercomputer grant of the "Stichting Nationale Computer Faciliteiten (NCF)".

References

1. M. J. Rice, *Phys. Lett.* **71A**, 152 (1979).
2. W. P. Su, J. R. Schrieffer, and A. J. Heeger, *Phys. Rev. Lett.* **42**, 1698 (1979).
3. W. P. Su, J. R. Schrieffer, and A. J. Heeger, *Phys. Rev.* **B22**, 2209 (1980); *Phys. Rev.* **B28**, 1138 (1983).
4. *Conjugated Conducting Polymers*, ed. H. Kiess (Springer-Verlag, Berlin, 1992).
5. A. J. Heeger, S. Kivelson, J. R. Schrieffer, and W.-P. Su, *Rev. Mod. Phys.* **60**, 781 (1988).
6. Y. Lu, *Solitons and Polarons in Conducting Polymers* (World Scientific, Singapore, 1988).
7. N. Suzuki, M. Ozaki, S. Etemad, A. J. Heeger, and A. G. Mac-Diarmid, *Phys. Rev. Lett.* **45**, 1209 (1980).
8. A. Feldblum, J. H. Kaufman, S. Etemad, and A. J. Heeger, *Phys. Rev.* **B26**, 815 (1982).
9. T.-C. Chung, F. Moreas, J. D. Flood, and A. J. Heeger, *Phys. Rev.* **B29**, 2341 (1984).
10. K. Maki and M. Nakahara, *Phys. Rev.* **B23**, 5005 (1981).
11. J. T. Gammel and J. A. Krumhansl, *Phys. Rev.* **B24**, 1035 (1981).

12. S. Kivelson, T.-K. Lee, Y. R. Lin-Liu, I. Peschel, and L. Yu, *Phys. Rev.* **B25**, 4173 (1982).
13. K. Kim, R. H. McKenzie, and J. W. Wilkins, *Phys. Rev. Lett.* **71**, 4015 (1993).
14. K. Michielsen, *Int. J. Mod. Phys.* **B7**, 2571 (1993).
15. L. Landau and E. Lifchitz, *Physique Statistique* (Édition Mir 1967).
16. H. De Raedt, *Proceedings of the Como Summer School on Monte Carlo and Molecular Dynamics*, eds. G. Ciccoto and K. Binder (in press).
17. W. von der Linden, *Phys. Rept.* **220**, 53 (1992).
18. R. Kubo, *J. Phys. Soc. Jpn.* **12**, 570 (1957).
19. W. Kohn, *Phys. Rev.* **133**, A171 (1964)
20. B. S. Shastry and B. Sutherland, *Phys. Rev. Lett.* **65**, 243 (1990).
21. D. J. Scalapino, S. R. White, and S.-C. Zhang, *Phys. Rev.* **B47**, 7995 (1993).
22. R. E. Peierls, *Quantum Theory of Solids* (Clarendon Press, Oxford, 1955).
23. J. Wagner, W. Hanke, and D. J. Scalapino, *Phys. Rev.* **B43**, 10517 (1991).
24. S. Hasegawa, M. Oku, M. Shimizu, and J. Tanaka, *Synth. Met.* **38**, 37 (1990).